# Spawning features of yellowfin and bigeye tuna in the Indian Ocean revealed by decadal Chinese longline observer data

Yang Wang<sup>1</sup>, Iker Zudaire<sup>2</sup>, Agurtzane Urtizberea<sup>2</sup>, Giancarlo M. Correa<sup>3</sup>, Jiangfeng Zhu<sup>1\*</sup>, Liang Chang<sup>4</sup>, Feng Wu<sup>1</sup>, Gorka Merino<sup>2</sup>

<sup>1</sup>College of Marine Living Resource Sciences and Management, Shanghai Ocean University, Shanghai 201306, China

<sup>4</sup>College of Oceanography and Ecological science, Shanghai Ocean University Shanghai 201306, China

\*Correspondence: Jiangfeng Zhu <jfzhu@shou.edu.cn>

Abstract: Reproductive dynamics of tropical tunas are critical for stock assessment and management in the Indian Ocean. Using over ten years of biological data collected from Chinese longline observers, this study analyzed the spatial and temporal patterns of spawning activity and environmental effects for bigeye tuna and yellowfin tuna. The estimated length at 50% maturity (L<sub>50</sub>) was 109.3 cm for bigeye and 106.2 cm for yellowfin tuna. Spawning seasons were identified as October–January for bigeye and October-March for yellowfin tuna. Spatial models revealed consistent high spawning probability areas in the equatorial western Indian Ocean (10°N-10°S, 40°-70°E). Sea surface temperature (SST) as the most important habitat factors showed the strongest positive influence on spawning probability for both species. These results complement histological studies and provide new evidence for spatially structured reproduction.

**Key words:** Reproductive biology; Spawning ground; Spatial distribution model; Yellowfin tuna; Bigeye tuna; Indian Ocean

#### 1. Introduction

Most studies aimed at describing maturation and spawning distributions in tunas have focused on ovaries, where scientists collected gonadal tissue samples and conducted precise histological analyses in the laboratory (Schaefer 2001; Zhu et al. 2008; Zudaire et al. 2013; Pacicco et al. 2023). This approach provides reliable accuracy in distinguishing developmental stages, from early vitellogenesis to imminent spawning and post-ovulatory states (Griffiths et al. 2019). Although histological analysis offers

<sup>&</sup>lt;sup>2</sup> AZTI, Marine Research, Basque Research and Technology Alliance (BRTA), Herrera Kaia, Portualdea z/g, 20110 Pasaia (Gipuzkoa), Spain <sup>3</sup> AZTI, Marine Research, Basque Research and Technology Alliance (BRTA), Txatxarramendi ugartea z/g, 48395 Sukarrieta (Bizkaia), Spain <sup>4</sup>College of Oceanography and Ecological science, Shanghai Ocean University,

high precision, it is constrained by several inherent limitations. Samples are typically collected from port landing or canneries (Diaha et al. 2016; Zudaire 2022), recreational fisheries (Pacicco et al. 2023), or through scientific observer programs (Zhu et al. 2008). As sample acquisition is costly, spatial coverage, temporal continuity, and overall sample sizes are generally limited. Moreover, samples especially from port landings and canneries generally lack fine-scale, georeferenced catch data required for robust spatial analyses, making it difficult to link spawning activity to specific environmental conditions and habitats (Kaplan et al. 2014; Wibawa et al. 2017).

In parallel, the implementation of the Regional Observer Scheme by IOTC contracting and cooperating non-contracting parties (CPCs) officially commenced in 2010 (IOTC Secretariat 2022). National and international fishery observer programs have emerged as a powerful source of fishery-dependent data. The program deploys trained technicians aboard commercial fishing vessels to collect biological information and catch statistics across operational areas (Cotter and Pilling 2007). The principal trade-off is that at-sea maturity assessment is performed by macroscopic staging of the gonads (West 1990). While faster and more feasible in an operational setting, macroscopic staging is known to be less accurate than histology (Costa 2009; Min et al. 2022). However, compared with laboratory sampling, observer programs generate substantially larger datasets with broader spatial coverage and linked to precise geographic coordinates (IOTC Secretariat 2023), thereby complementing laboratory-derived reproductive parameters and enabling analyses of spawning habitats and their environmental drivers.

Although yellowfin and bigeye tuna have been studied for several decades, the precise locations and environmental drivers of their spawning grounds in the Indian Ocean remain insufficiently resolved. Current knowledge of tuna spawning grounds in the Indian Ocean is based largely on empirical observations and environmental associations rather than systematic spatial analyses. For yellowfin tuna, spawning is generally assumed to occur in the equatorial western Indian Ocean, where sea surface temperatures exceed 24 °C (15°S - 10°N, west of 75°E) (Schaefer 2001; Zudaire et al. 2013). Spawning grounds for bigeye tuna in the Indian Ocean have not been clearly delineated. To address this research gap, we integrate a decade of georeferenced biological data from Chinese observer program with model-based analyses. The specific objectives of this study were: i) to estimate key reproductive parameters of yellowfin and bigeve tuna in the Indian Ocean and place these results in the context of previous researches, thereby assessing the effectiveness of observer-based datasets and contributing complementary information to existing knowledge; and ii) apply the sdmTMB spatial modeling framework to identify potential spawning habitats of these two species; and iii) to quantify the relationship between environmental variables and spawning probability. The findings will advances understanding of tuna reproductive ecology and will contribute to tuna fisheries management and conservation in the Indian Ocean.

#### 2. Materials and methods

# 2.1 Observer data collection and preparation

Biological and operational data were collected from the Chinese Observer Program on tuna longline vessels operating in the Indian Ocean, covering nearly 13 years from October 2012 to May 2025, daily (Figure 1). The dataset comprises detailed operational records, including fishing date, geographic position, hooks between floats, and the start and end times of setting and hauling, and etc. For each catch, biological information was recorded, including straight fork length (cm), processed weight (kg), sex, maturity stage, and gonad weight (g).

Female maturity was assessed macroscopically following a six-stage scale (West 1990; Diaha et al. 2016): (i) Stage 0: gonads are small, thread-like, and sex cannot be identified; (ii) Stage 1 - Immature: gonads are elongated and slender, but sex can be identified; (iii) Stage 2 - Early maturation: gonads are enlarged, but individual eggs are not visible to the naked eye; (iv) Stage 3 - Late maturation: gonads are enlarged, and individual eggs are visible to the naked eye; (v) Stage 4 - Fully mature: ovaries are highly enlarged, transparent or semi-transparent, easily separated from follicles, or loosely arranged in the ovarian lumen; (vi) Stage 5 - Spent: refers to individuals that have recently spawned or are in the late post-spawning stage.

# 2.2 Reproductive biology analysis

#### 2.2.1 Sex ratio

Sex ratio variation represents an important component of population reproductive dynamics (Morgan 2018). To evaluate sex ratio patterns, individuals were grouped into 5-cm length classes. For each class containing at least five specimens, the observed number of males and females was compared against the expected 1:1 ratio using a chi-square goodness-of-fit test:

$$x^{2} = \sum_{i=1}^{k} \frac{(O_{i} - E_{i})^{2}}{E_{i}}$$
 (1)

where  $O_i$  and  $E_i$  represent the observed and expected frequencies of males and females, respectively. The null hypothesis assumed no deviation from a 1:1 sex ratio, and p-values were used to assess the significance of departures from this expectation.

## 2.2.2 Length at 50% maturity

In histological analyses, ovaries in early vitellogenic stage including primary (Vtg1)

and secondary vitellogenesis (Vtg2) stages were considered mature, referred as functional maturity (Arocha et al. 2001; Diaha et al. 2016; Pacicco et al. 2023). Using functional maturity as the threshold to determine sexually mature fish is preferable since it guarantees that the fish will inevitably reproduce in the very short term (Pacicco et al. 2023; Urtizberea et al. 2024). To approximate this threshold in macroscopic staging, in this study, stage 3 was used as the maturity threshold. Length at 50% maturity (L<sub>50</sub>) of female were estimated using the non-linear logistic equation (Saborido-Rey and Junquera 1998; Zudaire et al. 2013; Pacicco et al. 2023):

$$P_L = \frac{1}{1 + \rho^{-(\alpha + \beta L)}} \tag{2}$$

where  $P_L$  is the proportion of mature females (stages 3-5) in length class L, and  $\alpha$  and  $\beta$  are parameters represent the intercept and the slope of the logistic equation, respectively. Model parameters were estimated using a generalized linear model with binomial error distribution and a logit link. L<sub>50</sub> was estimated as the ratio of the parameters ( $-\alpha\beta^{-1}$ ). Confidence intervals and standard errors for L<sub>50</sub> were derived by applying the delta method to the variance-covariance matrix of the estimated parameters. Significance of the length-maturity relationship was assessed using Wald tests for model coefficients.

# 2.2.3 Spawning seasonality

The gonad somatic index (GSI) was used to identify the spawning status and season. As the weights recorded by observers represented processed weights (gilled, gutted, and tailed), the GSI was estimated by fork length as follows (Matsumoto and Miyabe 2002; Nootmorn et al. 2005; Zhu et al. 2008):

$$GSI = \frac{W}{FL^3} \times 10^4 \tag{3}$$

where W is gonad weight (g); FL is the straight fork length (cm). GSI distributions were compared among maturity stages to evaluate staging reliability, and monthly mean GSI values were plotted to infer spawning seasonality. Given that the dataset covers a wide latitudinal range across the Indian Ocean, we limited the estimation of monthly mean GSI to the tropical domain (40°–70°E, 20°S–15°N). This restriction minimizes the influence of non-reproductive individuals occurring in temperate waters and ensures that the calculated seasonal pattern reflects the reproductive dynamics within the core spawning habitat.

# 2.3 Spatial modeling of spawning grounds

## 2.3.1 Model structure

The sdmTMB framework (Anderson et al. 2022) was applied to model the spatial

distribution of spawning grounds. This approach implements spatiotemporal generalized linear mixed models (GLMM) allowing explicit modeling of spatial autocorrelation among observations. A Gaussian random field (GRF) was used to represent this latent spatial dependence, where spatial random effects are assumed to follow a multivariate normal distribution with mean vector  $\mu = [\mu(s_1), \ldots, \mu(s_n)]$  and spatially structured covariance matrix  $\Sigma$  (Blangiardo and Cameletti 2015; Correa et al. 2025). As GRFs require dense  $n \times n$  covariance matrix factorization, their direct implementation is computationally demanding (Hebert et al. 2024). The sdmTMB applied the stochastic partial differential equations (SPDEs) approach to reduce the computational costs.

In this study, we constructed the mesh using the SPDE approach, with triangles covering the study area and a minimum allowed edge length (cutoff) of 0.5°. Due to the sparse records in some year as reflected in the observer data (e.g. during Covid-19 period), temporal random fields were not included in the sdmTMB model. Therefore, the GLMM with spatial Gaussian random fields can be written as (Anderson et al. 2022; Hebert et al. 2024; Correa et al. 2025):

$$\mathbb{E}[y_s] = \mu_s,$$
  

$$\mu_s = g^{-1}(\eta_s),$$
  

$$\eta_s = X_s \beta + V_i + \omega_s$$
(4)

where the expected value  $\mathbb{E}[.]$  of an observation y at coordinates in space s is defined as the mean  $\mu_s$ , which is the result of an inverse link function  $g^{-1}$  applied to a linear predictor  $\eta_s$ .  $X_s$  is the model matrix of fixed effects with coefficients  $\beta$ .  $V_i$  represents each vessel random effects. And  $\omega_s$  denotes the spatial random field capturing spatially correlated variation not explained by the fixed effects in the model:

$$\omega \sim \text{MVNormal}(0, \Sigma_{\omega})$$
 (5)

where  $\sum_{\omega}$  specifies the covariance of the spatial random field, modeled using a Matérn covariance function that determines how spatial dependence decays with distance.

In this research, following the reproductive classification of tuna (Zudaire et al. 2013; Diaha et al. 2016), maturity stages 3 and 4 were coded as spawning (1), and the remaining stages as non-spawning (0). The response variable y was therefore modeled as a binomial distribution using a logic link function.

### 2.3.2 Covariates

Covariates were classified into two categories: habitat and catchability covariates (Thorson 2019). Habitat covariates represent environmental factors that influence the true distribution or abundance of the population, whereas catchability covariates

primarily affect the probability of observation. Given that the observer dataset was fishery-dependent, this classification helped disentangle biological processes from sampling effects. Predictions of spawning probability were conditioned only on density covariates.

Table 1 shows all the covariates explored in this study. The variable *month* was included to account for potential seasonal variability in fishing activities and spawning behavior. For the catchability covariates, the effect of different vessels was included as a random factor to capture vessel-specific differences in fishing practices and observers' behavior. The hooks between floats (HBF) variable was incorporated as a proxy for fishing depth, as it determines the vertical distribution of hooks and consequently influences the likelihood of encountering spawning individuals. In addition, given that yellowfin tuna are reported to spawn mainly at night (Schaefer and Fuller 2022), the proportion of night-time operation was calculated for each set. This proportion was derived by computing the midpoint time between gear deployment and retrieval, and determining whether it occurred within local nighttime hours based on daily nautical sunrise and sunset times.

Based on the two main hypotheses have been proposed to explain the global distribution of tuna spawning grounds: (1) that spawning is constrained by temperature and generally occurs in waters warmer than 24 °C (Schaefer 2001), and (2) that spawning is associated with mesoscale oceanographic features such as fronts and eddies (Reglero et al. 2014). Accordingly, sea surface temperature (SST) and eddy kinetic energy (EKE) were included as key explanatory habitat covariates. As a substantial number of sampling stations were located near islands, distance to coast (DTC) and total depth (TD) were also incorporated. Additional environmental variables with potential relevance to reproductive activity included sea surface height (SSH), sea surface salinity (SSS), chlorophyll-a concentration (Chl-a), mixed layer depth (MLD), dissolved oxygen (DO), and the Indian Ocean Dipole Mode Index (DMI). The SST, SSS, MLD and SSH downloaded from Multi Observation Global Ocean ARMOR3D database

(https://data.marine.copernicus.eu/product/MULTIOBS\_GLO\_PHY\_TSUV\_3D\_MY\_NRT\_015\_012/description), with 0.25° spatial resolution and weekly temporal resolution. EKE came from Copernicus Climate Service (https://data.marine.copernicus.eu/product/SEALEVEL\_GLO\_PHY\_CLIMATE\_L4\_MY\_008\_057/description), with 0.25° spatial resolution and daily temporal resolution. DTC is the distances to the neatest coastline (include major islands), which downloaded from Ocean Color program with a 0.04 spatial degree (https://oceancolor.gsfc.nasa.gov/resources/docs/distfromcoast/). TD from the gridded bathymetry datasets with 0.0042° spatial resolution (https://www.gebco.net/data-products/gridded-bathymetry-data). DO from the Global Ocean Biogeochemistry Hindcast dataset with 0.25 spatial resolution and daily temporal resolution (https://data.marine.copernicus.eu/product/GLOBAL\_MULTIYEAR\_BGC\_001\_029/description). Chl-a downloaded from the Ocean Color daily data with 0.036° spatial

resolution (https://oceandata.sci.gsfc.nasa.gov/l3/). And the DMI from NASA with weekly temporal resolution

(https://podaac.jpl.nasa.gov/dataset/NASA\_SSH\_IOD\_INDICATOR). Variance inflation factor (VIF) values lower than 5 was used to test the multicollinearity among independent variables.

# 2.3.3 Model selection and diagnostic

The modeling process began with a baseline model that included only the month, vessel (as a random effect), and the spatial random field. Habitat and catchability covariates were then added sequentially. The final model was selected based on the lowest Akaike Information Criterion (AIC) value. Based on the exploratory analysis, model assuming linear relationships between the response variable and continuous covariates provided the best fit, so nonlinear terms were not included. Covariates with non-significant effects (p > 0.05) were removed to obtain the most parsimonious model.

Model diagnostics were first assessed using the built-in tools of the sdmTMB package, which check model convergence, parameter identifiability, gradient magnitude, and the Hessian matrix to ensure stable maximum likelihood estimation. Further diagnostic evaluation was conducted using the *DHARMa R* package, which generates standardized (quantile) residuals through simulation-based methods for generalized linear mixed models. Two diagnostic plots were examined: (1) a quantile-quantile (Q-Q) plot to detect deviations of residuals from the expected distribution, and (2) a plot of residuals versus fitted values to identify patterns or potential outliers. In addition, spatial autocorrelation in the randomized quantile residuals was evaluated using Moran's I statistic (Moran 1950) to confirm that no significant spatial structure remained in the residuals.

## 2.3.4 Model prediction

Spawning probability was predicted for the study region using a "predict-then-aggregate" approach. Predictions were generated on a 1° grid, where catchability covariates were fixed at their mean values and habitat covariates were assigned according to environmental conditions at each grid centroid. Model predictions were limited to grid cells containing observed data. To further examine temporal variation, monthly spawning probability was predicted for the area with the highest sampling density (40°-70°E, 20°S-10°N) by substituting observed habitat values for each 1° grid cell.

To quantify the effects of individual environmental variables, partial effect plots were generated for all continuous covariates included in the final model. For each variable, marginal predictions were computed across its observed range while holding other covariates constant at their mean values. The resulting effects were visualized using

the *ggeffects* package, and variables were ordered by the magnitude of their estimated coefficients to indicate relative importance.

#### 3. Results

#### 3.1 Sex ratio

The sex ratio of both bigeye tuna and yellowfin tuna varied significantly with fork length increase. In both species, females predominated in the smaller size classes, whereas the proportion of males increased steadily with size. For bigeye tuna, the proportion of males exceeded 0.5 at fork lengths greater than approximately 160 cm, and this difference was statistically significant ( $\chi^2$  test, p < 0.05) (Figure 2). Similarly, yellowfin tuna showed a higher proportion of females below 150 cm and a predominance of males at lengths above 160 cm (p < 0.05) (Figure 3). These results indicate a size-dependent sex ratio pattern, with larger individuals being predominantly male in both species.

## 3.2 Length at maturity

Logistic regression models were fitted to the proportion of mature females by fork length to estimate the parameters  $\alpha$  (intercept) and  $\beta$  (slope) of the maturity ogive (Table 2). Both parameters were highly significant according to Wald tests (p < 0.001), indicating a strong positive relationship between maturity and length for both species. For bigeye tuna, the estimated parameters were  $\alpha$  equals -16.83 and  $\beta$  equals 0.15, corresponding to a L50 of 109.3 cm (95% CI: 108.5–110.1 cm). For yellowfin tuna,  $\alpha$  equals -15.95 (SE = 0.47) and  $\beta$  equals 0.150 (SE = 0.005), yielding an L50 of 106.2 cm (95% CI: 105.6–106.8 cm). The fitted courves (Figures 4 - 5) closely matched the observed data points, with only slight deviations observed in the smallest length classes.

## 3.3 Spawning season

GSI increased progressively with maturity stage in both species, reaching the highest values at stage 4 and decreasing in stage 5 (Figures 6). Monthly variations in the mean GSI revealed distinct seasonal patterns (Figure 7). For bigeye tuna, GSI increased gradually from September, peaked between October and January, and declined thereafter. For yellowfin tuna, GSI values began to rise in September, remained elevated from October to March, and decreased during April to Augus. Therefore, the spawning season for bigeye tuna was identified as October to January, for yellowfin tuna is October to March.

#### 3.4 Potential spawning ground

#### 3.4.1 Model diagnostic

Collinearity diagnostics showed that DO was strongly collinear with SST for bigeye tuna, and removed this variable prior to model selection. For yellowfin tuna, there is no collinearity between covariates (Table 3). Model selection based on AIC indicated that models incorporating both catchability and habitat covariates provided the best fit for both species (Table 4). After exploring for variable correlations, the retained covariates for bigeye tuna were SST, DTC, MLD, DMI, EKE, SSH, and TD, while for yellowfin tuna the final model included SST, DTC, MLD, DMI, EKE, SSS, and DO. The proportion of nighttime sets showed no significant correlation with spawning probability in either species and was therefore excluded.

The DHARMa Q-Q plot of bigeye tuna showed that residuals closely followed the expected uniform distribution (KS test: p = 0.134), and no outliers were detected (p = 0.926). Although the dispersion test suggested significant overdispersion (p < 0.001), the residuals versus predicted values displayed only a weak positive trend, indicating no substantial systematic deviation (Figure 8). The diagnostic results were almost consistent for yellowfin tuna (Figure 9). Moran's I p values for bigeye tuna and yellowfin tuna were 0.343 and 0.661, respectively (Table 4). Residuals randomly distributed in the study region indicating no significant spatial autocorrelation in model residuals (Figure 8, 9).

# 3.4.2 Potential spawning ground

Model predictions revealed distinct spatial patterns of spawning probability for bigeye tuna and yellowfin tuna. For bigeye tuna (Figure 10), the spatial random field (Figure 10B) showed strong positive deviations concentrated in the equatorial western Indian Ocean, particularly between 50°E-70°E and 0-10°S, indicating spatial clustering of high spawning probability not fully explained by environmental covariates. The overall prediction map (Figure 10C) highlighted a clearly defined spawning ground within this region, extending slightly eastward along the equatorial zone and weakening toward the southern and coastal waters. However, yellowfin tuna exhibited a more diffuse spatial pattern (Figure 11). The spatial random field (Figure 11B) displayed weak and spatially scattered positive deviations, suggesting less pronounced spatial aggregation. The predicted spawning probability (Figure 11C) indicated broad but patchy areas of potential spawning activity across the central tropical western Indian Ocean, mainly between 45°E-70°E and 5°N-10°.

The intensity of spawning probability showed distinct seasonal fluctuations for bigeye tuna, with elevated values observed from October to January, corresponding to the main spawning season identified from GSI analysis. Lower probabilities occurred during June to August, indicating a reduction in reproductive activity during the austral winter period (Figure 12). For yellowfin tuna, spatial patterns were more homogeneous, with moderate spawning probabilities maintained across the central tropical western Indian Ocean (Figure 13).

#### 3.5 Partial effects of habitat covariates

The partial effects show that sea surface temperature (SST) is the most influential factor for the spawning probability of both species (Figure 14,15). For yellowfin tuna, spawning probability increases sharply with SST, indicating that spawning mainly occurs in warm tropical waters above around 25°C. For bigeye tuna, the relationship is also positive but weaker, suggesting that this species prefers slightly cooler temperatures, around 24-28 °C. Neither curve shows a decline at high SST, probably because the temperature range in our data did not exceed the upper thermal limits for spawning activity. Other environmental effects are consistent with their ecology: bigeye spawning probability increases with distance from the coast, reflecting its oceanic nature, whereas yellowfin shows higher probability in nearshore or island-associated waters. Both species prefer shallower mixed layers and show weak positive effects of eddy kinetic energy, indicating that moderately dynamic environments may favor spawning. Positive IOD events had weekly negative influence on both species.

## 4 Summary

The results derived from the Chinese longline observer dataset are broadly consistent with previous findings based on histological analyses, demonstrating the reliability of at-sea observer data for reproductive studies. Compared with port-sampling programs, observer-based sampling provides spatially extensive and temporally continuous biological information, which can complement conventional datasets and improve the estimation of reproductive parameters such as maturity ogives and spawning seasonality.

The estimated length at 50% maturity (L<sub>50</sub>) for bigeye tuna (109.3 cm) closely matches the value currently used in stock assessments (110.9 cm; Shono et al., 2009), supporting the robustness of our maturity classification. In contrast, the L<sub>50</sub> for yellowfin tuna (106.2 cm) was slightly higher than the value applied in recent assessments (101.7 cm). This difference may be attributed to spatial variation in reproductive timing, as yellowfin tuna near the equator have been reported to mature earlier (Itano 2000). Moreover, observer-based sampling may introduce uncertainty due to potential misclassification of gonadal stages at sea.

Spawning activity was found to be seasonal, with bigeye tuna spawning mainly from October to January and yellowfin tuna from October to March. These periods correspond to the warm season in the equatorial Indian Ocean. The identified seasonality agrees with observations from previous studies (Nootmorn et al. 2005; Zhu et al. 2008; Zudaire et al. 2013).

Spatial modeling revealed consistent high spawning probability areas in the equatorial and western Indian Ocean, particularly between 10°N-10°S and 40°-70°E. The

overlapping spawning habitats of yellowfin and bigeye tunas may reflect their shared environmental preferences and life-history interactions, as juvenile bigeye are known to form mixed schools with juvenile yellowfin and skipjack tunas (Pickerell 2024). The strong positive effect of SST on spawning probability observed in both species reinforces its role as a primary environmental driver regulating tuna reproduction, consistent with previous studies emphasizing temperature as a key determinant of spawning habitat suitability (Schaefer 2001).

From a fisheries management perspective, the identification of spatially structured spawning habitats suggests potential implications for stock assessment and management. The presence of concentrated spawning areas, particularly for bigeye tuna, supports the need to consider spatial population structure when defining assessment units. Seasonal patterns in spawning activity may also influence the availability of mature individuals to fisheries, thereby affecting estimates of spawning biomass and recruitment timing in stock assessment models. Incorporating such temporal and spatial variability into future assessments could help improve the accuracy of reproductive potential estimates and enhance the management of tropical tuna fisheries under changing environmental conditions.

#### 5 References

- Anderson SC, Ward EJ, English PA, Barnett LAK (2022) sdmTMB: an R package for fast, flexible, and user-friendly generalized linear mixed effects models with spatial and spatiotemporal random fields. 2022.03.24.485545
- Arocha F, Lee DW, Marcano LA, Marcano JS (2001) Update information on the spawning of yellowfin tuna, *Thunnus Albacares*, in the western central Atlantic. International Convention for the Conservation of Atlantic Tunas
- Blangiardo M, Cameletti M (2015) Spatio-temporal models. In: Spatial and Spatio-temporal Bayesian Models with R-INLA. John Wiley & Sons, Ltd, pp 235–258
- Correa G, Kaplan D, Uranga J, et al (2025) Standardized catch per unit effort of bigeye tuna in the Indian Ocean for the European purse seine fleet operating on floating objects. Indian Ocean Tuna Commission, onlie
- Costa AM (2009) Macroscopic vs. microscopic identification of the maturity stages of female horse mackerel. ICES Journal of Marine Science 66:509–516. https://doi.org/10.1093/icesjms/fsn216
- Cotter AJR, Pilling GM (2007) Landings, logbooks and observer surveys: improving the protocols for sampling commercial fisheries. Fish and Fisheries 8:123–152. https://doi.org/10.1111/j.1467-2679.2007.00241.x
- Diaha NC, Zudaire I, Chassot E, et al (2016) Annual monitoring of reproductive traits of female yellowfin tuna (*thunnus albacares*) in the eastern Atlantic Ocean. International Convention for the Conservation of Atlantic Tunas
- Griffiths S, Zischke M, van der Velde T, Fry G (2019) Reproductive biology and estimates of length and age at maturity of longtail tuna (*Thunnus tonggol*) in Australian waters based

- on histological assessment. Marine and Freshwater Research 70:1419–1426. https://doi.org/10.1071/MF18469
- Hebert NE, Sameoto JA, Keith DM, et al (2024) Comparing spatiotemporal species distribution models: A case study of a Scotian Shelf sea cucumber (*Cucumaria frondosa*). Ecosphere 15:e4822. https://doi.org/10.1002/ecs2.4822
- IOTC Secretariat (2022) Regional Observer Scheme. Indian Ocean Tuna Commission, Seychelles
- IOTC Secretariat (2023) ROS Data Standards. Indian Ocean Tuna Commission, Seychelles
- Itano D (2000) The Reproductive Biology of Yellowfin Tuna (*Thunnus albacares*) in Hawaiian Waters and the Western Tropical Pacific Ocean: Project Summary. Joint Institute for Marine and Atmospheric Research Report 00–328:
- Kaplan DM, Chassot E, Amandé JM, et al (2014) Spatial management of Indian Ocean tropical tuna fisheries: potential and perspectives. ICES Journal of Marine Science 71:1728–1749. https://doi.org/10.1093/icesjms/fst233
- Matsumoto T, Miyabe N (2002) Preliminary report on the maturity and spawning of bigeye tuna *Thunnus Obesus* in the central Atlantic Ocean. The International Commission for the Conservation of Atlantic Tunas
- Min MA, Head MA, Cope JM, et al (2022) Limitations and applications of macroscopic maturity analyses: a comparison of histological and visual maturity for three west coast groundfish species. Environ Biol Fish 105:193–211. https://doi.org/10.1007/s10641-021-01208-2
- Moran PAP (1950) Notes on Continuous Stochastic Phenomena. Biometrika 37:17–23. https://doi.org/10.2307/2332142
- Morgan MJ (2018) Understanding biology to improve advice for fisheries management. ICES J Mar Sci 75:923–931. https://doi.org/10.1093/icesjms/fsx229
- Nootmorn P, Yakoh A, Kawises K (2005) Reproductive biology of yellowfin tuna in the eastern Indian Ocean. Indian Ocean Tuna Commission, Phuket, Thailand
- Pacicco AE, Brown-Peterson NJ, Murie DJ, et al (2023) Reproductive biology of yellowfin tuna (*Thunnus albacares*) in the northcentral U.S. Gulf of Mexico. Fisheries Research 261:106620. https://doi.org/10.1016/j.fishres.2023.106620
- Pickerell T (2024) Tuna sustainability. In: Dikeman M (ed) Encyclopedia of Meat Sciences (Third Edition). Elsevier, Oxford, pp 66–78
- Reglero P, Tittensor D, Álvarez-Berastegui D, et al (2014) Worldwide distributions of tuna larvae: revisiting hypotheses on environmental requirements for spawning habitats.

  Marine Ecology Progress Series 501:207–224. https://doi.org/10.3354/meps10666
- Saborido-Rey F, Junquera S (1998) Histological assessment of variations in sexual maturity of cod (*Gadus morhua L.*) at the Flemish Cap (north-west Atlantic). ICES Journal of Marine Science 55:515–521. https://doi.org/10.1006/jmsc.1997.0344
- Schaefer KM (2001) Reproductive biology of tunas. San Diego, California
- Schaefer KM, Fuller DW (2022) Spatiotemporal variability in the reproductive biology of yellowfin tuna (*Thunnus albacares*) in the eastern Pacific Ocean. Fisheries Research 248:106225. https://doi.org/10.1016/j.fishres.2022.106225
- Thorson JT (2019) Guidance for decisions using the Vector Autoregressive Spatio-Temporal (VAST) package in stock, ecosystem, habitat and climate assessments. Fisheries

- Research 210:143–161. https://doi.org/10.1016/j.fishres.2018.10.013
- Urtizberea A, Correa G, Langley A, et al (2024) Stock assessment of yellowfin tuna in the Indian Ocean. Indian Ocean Tuna Commission, Seychell
- West G (1990) Methods of Assessing Ovarian development in Fishes: a Review. Marine and Freshwater Research 41:199–222. https://doi.org/10.1071/mf9900199
- Wibawa TA, Lehodey P, Senina I (2017) Standardization of a geo-referenced fishing data set for the Indian Ocean bigeye tuna, Thunnus obesus (1952–2014). Earth System Science Data 9:163–179. https://doi.org/10.5194/essd-9-163-2017
- Zhu G, Xu L, Zhou Y, Song L (2008) Reproductive biology of yellowfin tuna *T. albacares* in the west-central Indian Ocean. Journal of Ocean University of China 7:327–332. https://doi.org/10.1007/s11802-008-0327-3
- Zudaire I, Artetxe-Arrate I, Farley J, et al (2022) Preliminary estimates of sex ratio, spawning season, batch fecundity and length at maturity for Indian Ocean bigeye tuna. Indian Ocean Tuna Commission, Online
- Zudaire I, Murua H, Grande M, Bodin N (2013) Reproductive potential of Yellowfin Tuna (*Thunnus albacares*) in the western Indian Ocean. Fishery Bulletin 111:252–264. https://doi.org/10.7755/fb.111.3.4

# 6 Figures

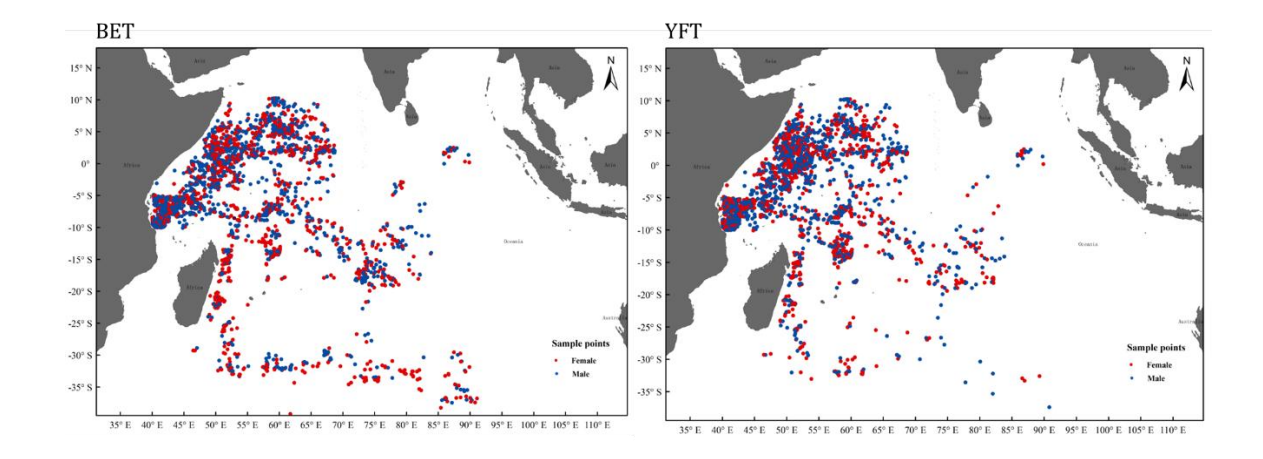


Figure 1 Spatial distribution of observer sampling records for bigeye tuna and yellowfin tuna in the Indian Ocean from 2012 to 2025. Red points indicate female individuals, and blue points indicate male individuals.

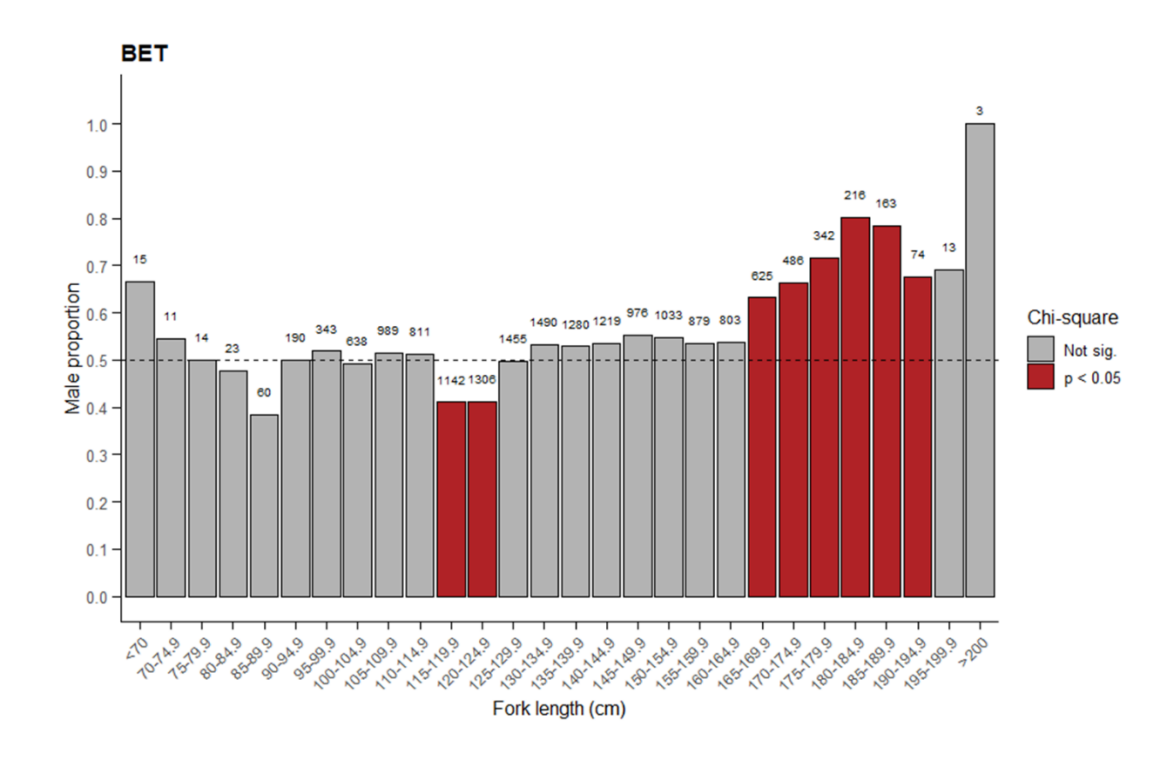


Figure 2 Proportion of males by fork length class for bigeye tuna in the Indian Ocean. Red bars indicate length classes where the sex ratio differed significantly from parity (p < 0.05), and grey bars indicate non-significant differences.

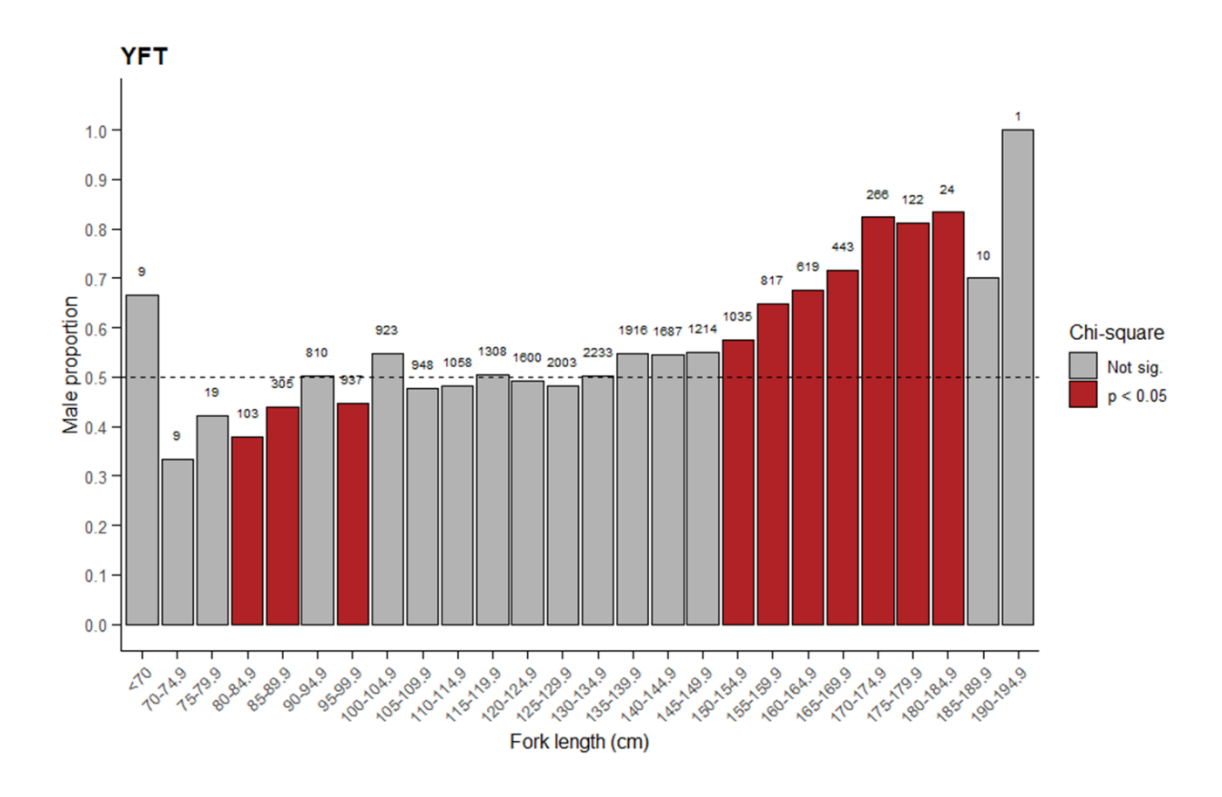


Figure 3 Proportion of males by fork length class for yellowfin tuna in the Indian Ocean. Red bars indicate length classes where the sex ratio differed significantly from parity (p < 0.05), and grey bars indicate non-significant differences.

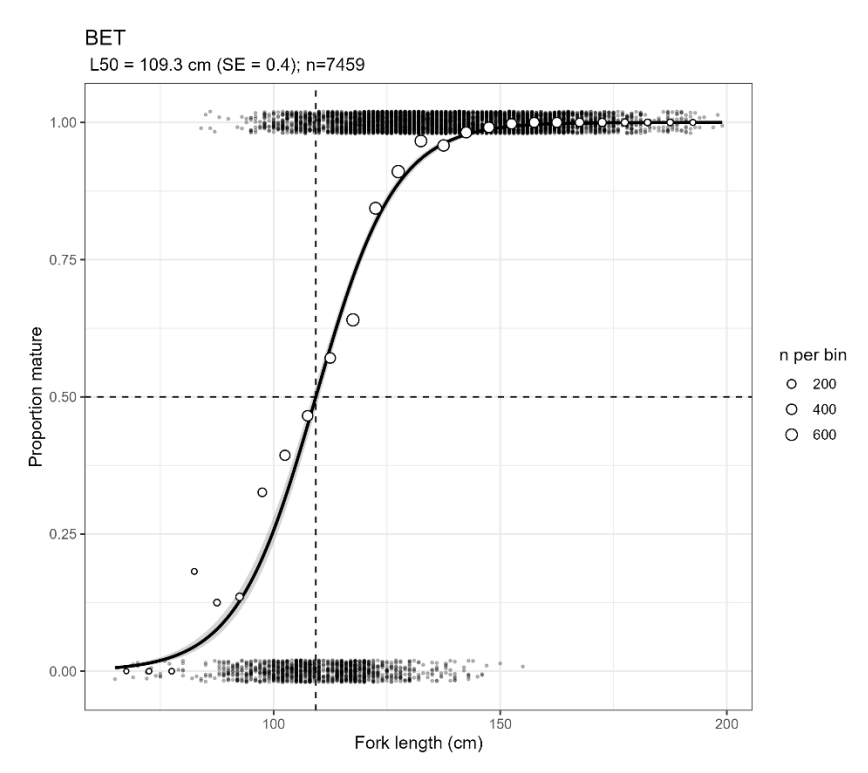


Figure 4 Maturity ogive for female bigeye tun in the Indian Ocean. Open circles represent binned proportions of mature individuals by fork length. Black dots at 0 and 1 represent individual observations classified as no spawn and spawn, respectively. The dashed lines indicate 50% maturity (horizontal) and the estimated L50 (vertical).

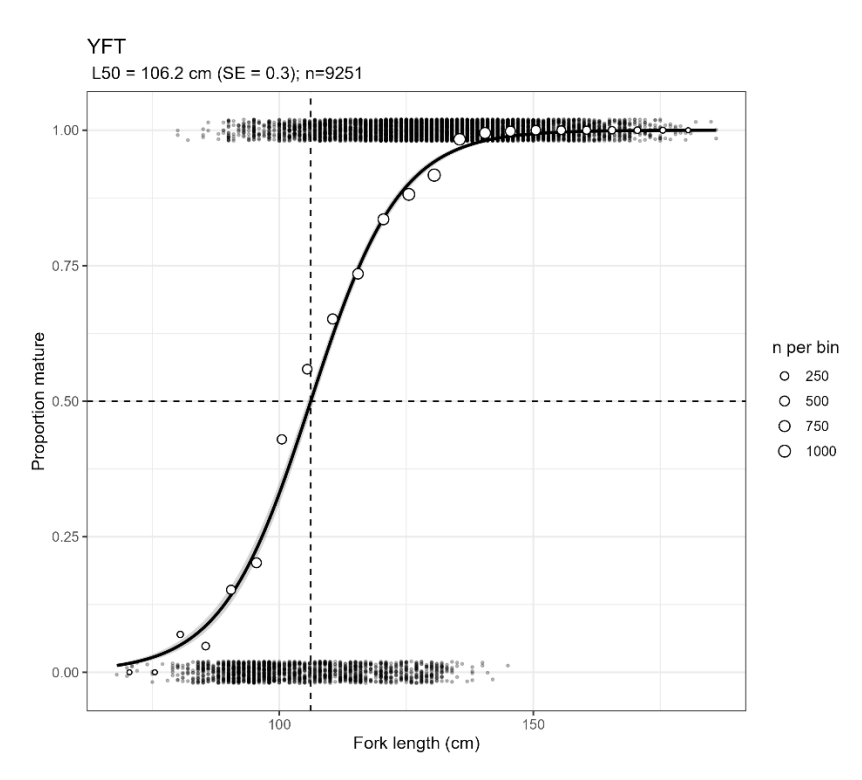


Figure 5 Maturity ogive for female yellowfin tun in the Indian Ocean. Open circles represent binned proportions of mature individuals by fork length. Black dots at 0 and 1 represent individual observations classified as no spawn and spawn, respectively.

The dashed lines indicate 50% maturity (horizontal) and the estimated L<sub>50</sub> (vertical).

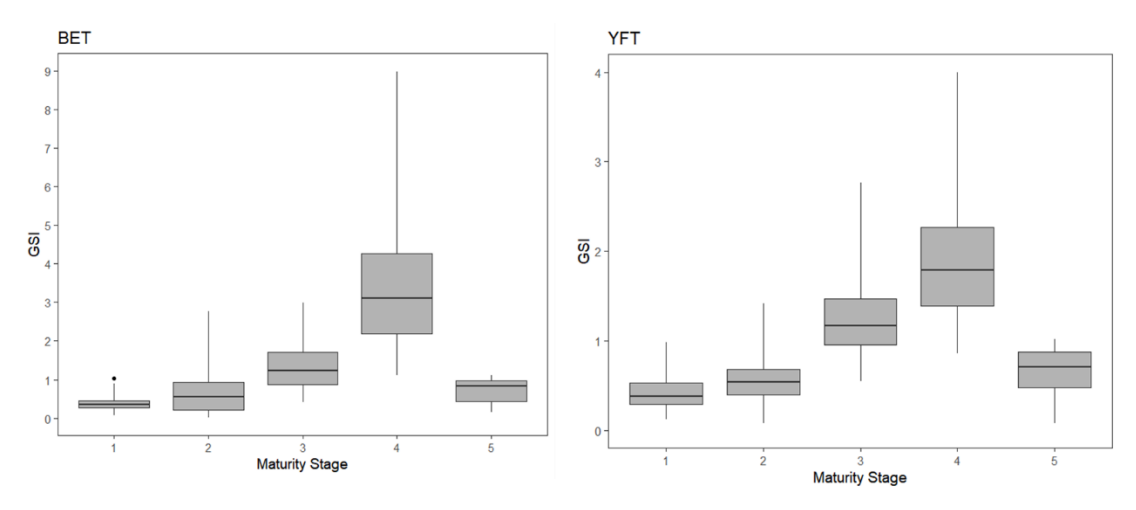


Figure 6: Boxplots of the gonadosomatic index (GSI) by maturity stage for female bigeye tuna and yellowfin tuna in the Indian Ocean. BET: bigeye tuna; YFT: yellowfin tuna.

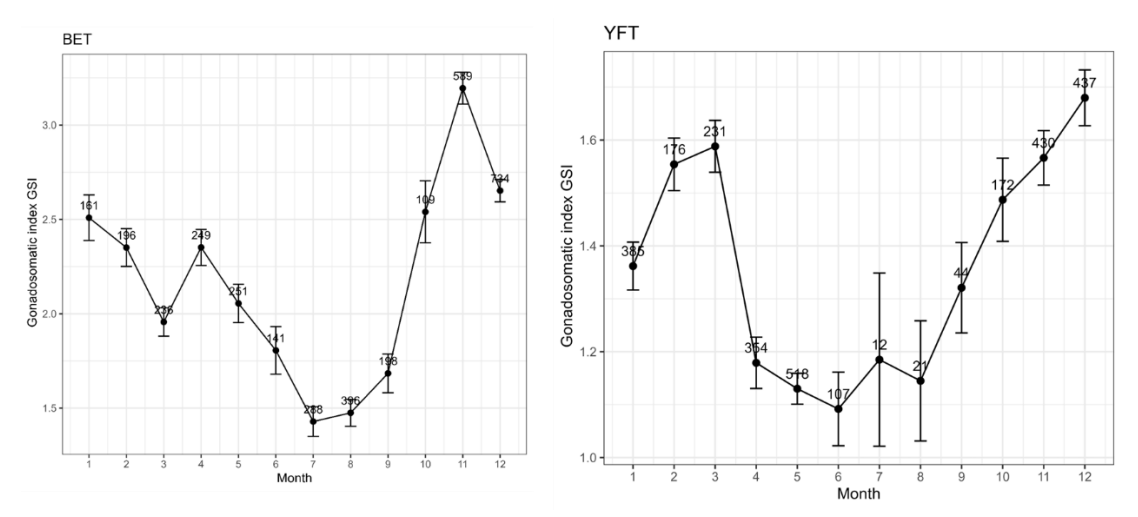


Figure 7: Monthly variation in mean gonadosomatic index (GSI  $\pm$  SE) for female bigeye tuna and yellowfin tuna in the tropical Indian Ocean (40° - 70°E, 20°S - 15°N). Numbers above points indicate sample size per month.

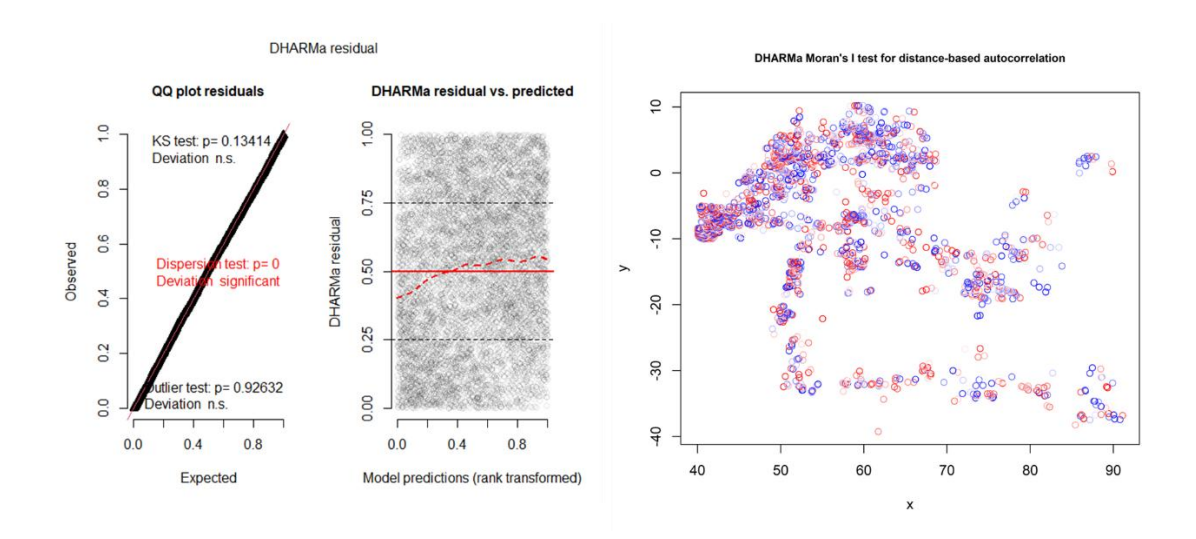


Figure 8: Simulation-based randomized-quantile residuals for the bigeye model. QQ-plot detects overall deviations from the expected distribution, by default with added tests for correct distribution (KS test), dispersion and outliers. Residual plot shows the residuals against the predicted value (left). Moran's I plots shows the spatial distribution of residuals (right). Red points: positive residuals. Blue points: negative residuals.

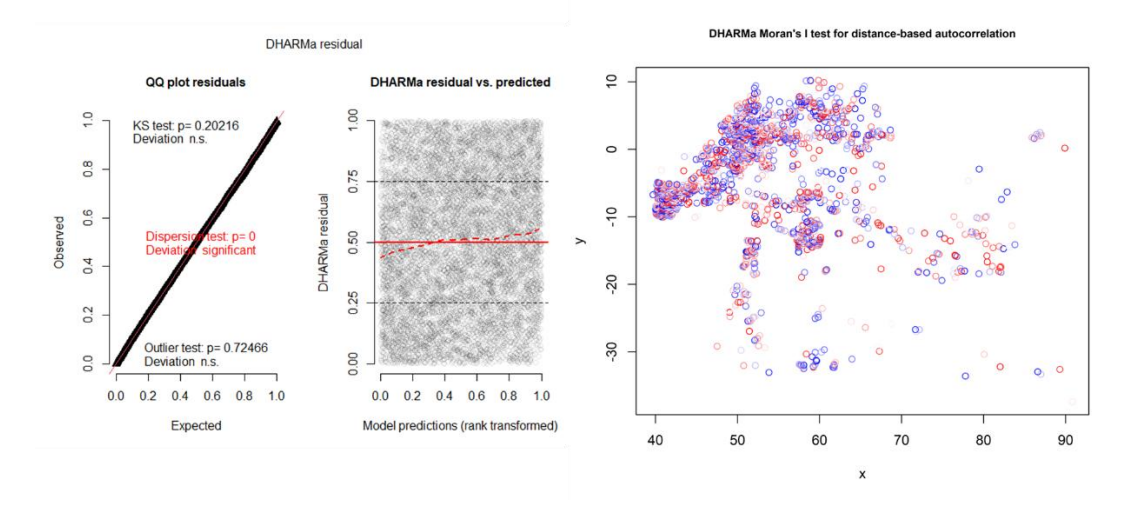


Figure 9: Simulation-based randomized-quantile residuals for the bigeye model. QQ-plot detects overall deviations from the expected distribution, by default with added tests for correct distribution (KS test), dispersion and outliers. Residual plot shows the residuals against the predicted value (left). Moran's I plots shows the spatial distribution of residuals (right). Red points: positive residuals. Blue points: negative residuals.

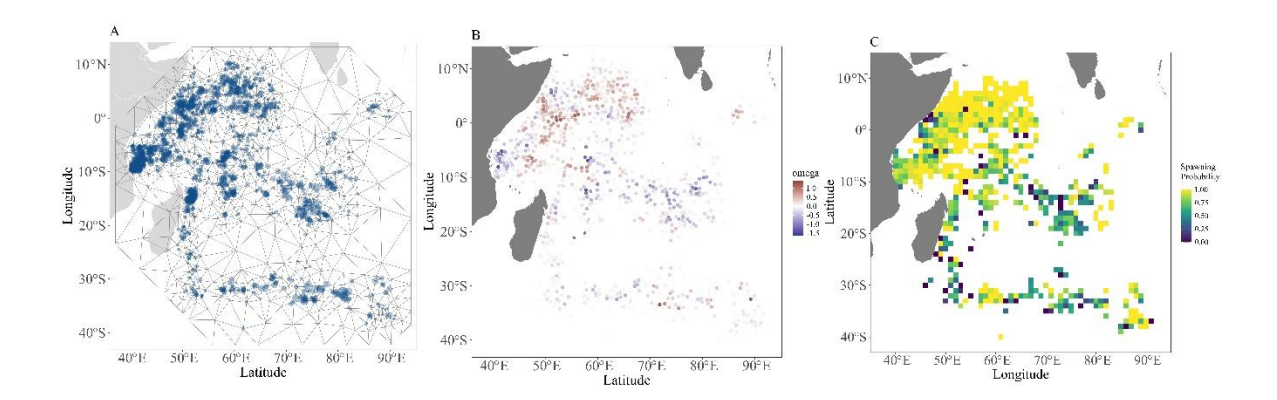


Figure 10: Model results for bigeye tuna. A: SPDE mesh (lines) combined with observations (points). B: Spatial random field: these values are shown in link (log) space and represent spatially correlated deviations that are not accounted for by the covariates. C: Overall prediction: these estimates represent the combination of all fixed and random effects.

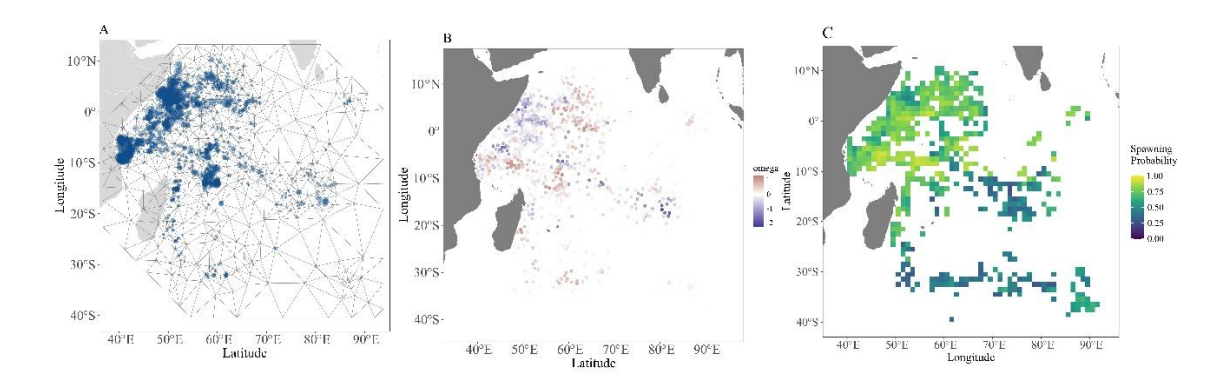


Figure 11: Model results for yellowfin tuna. A: SPDE mesh (lines) combined with observations (points). B: Spatial random field: these values are shown in link (log) space and represent spatially correlated deviations that are not accounted for by the covariates. C: Overall prediction: these estimates represent the combination of all fixed and random effects.

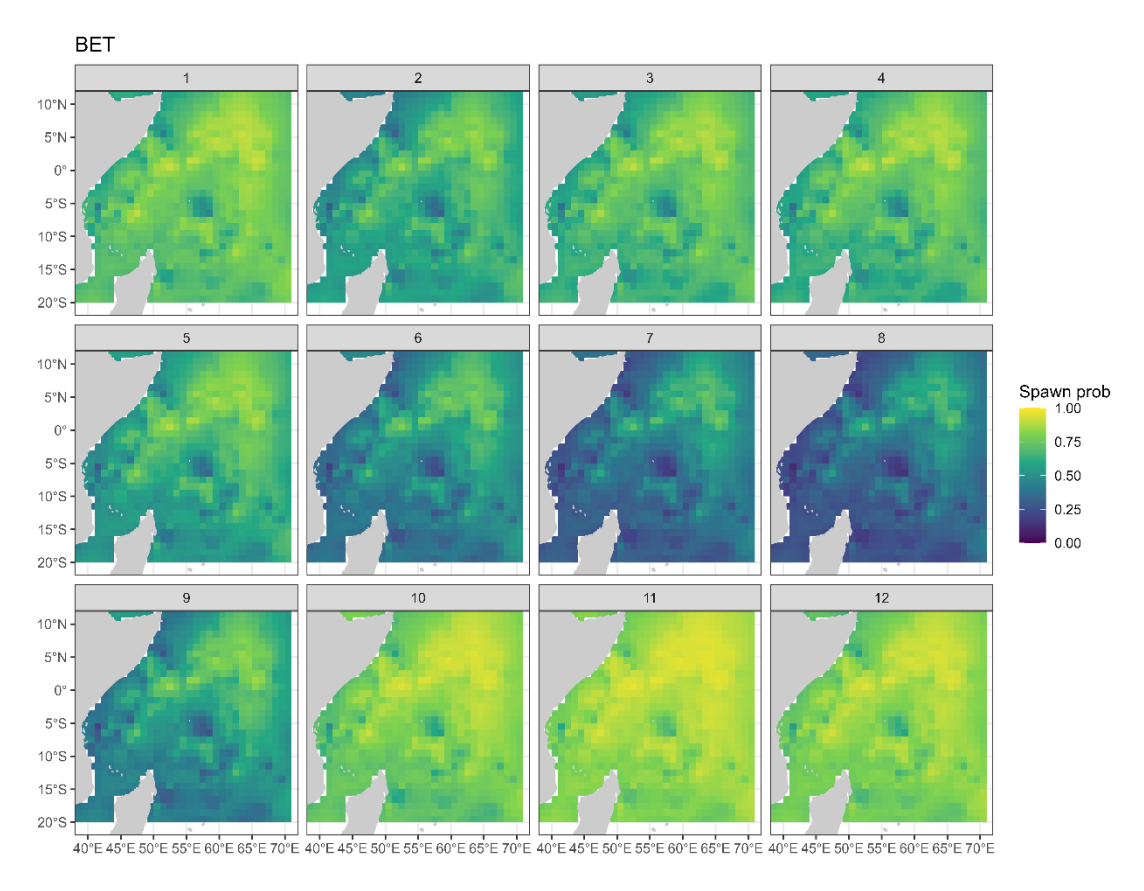


Figure 12 Monthly spawning probability for bigeye tuna in the tropical Indian Ocean.

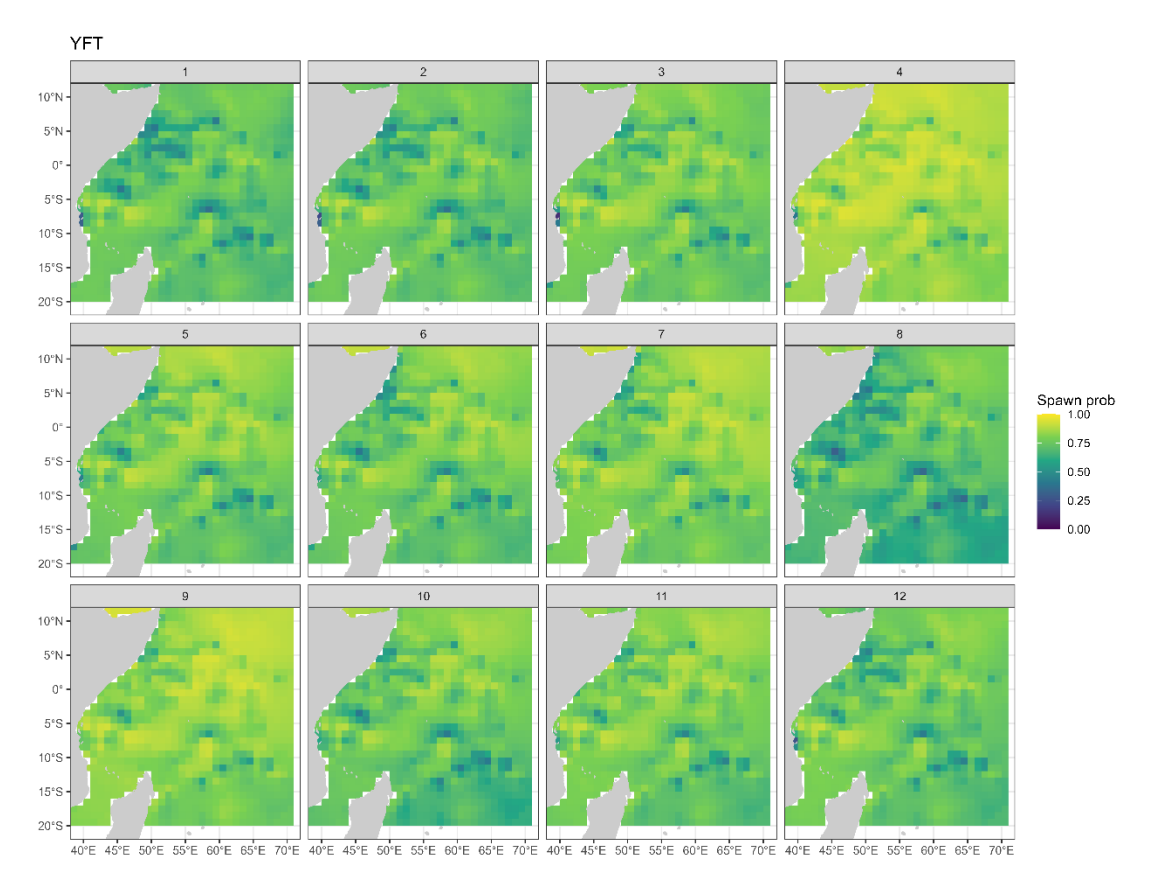


Figure 13 Monthly spawning probability for yellowfin tuna in the tropical Indian Ocean.

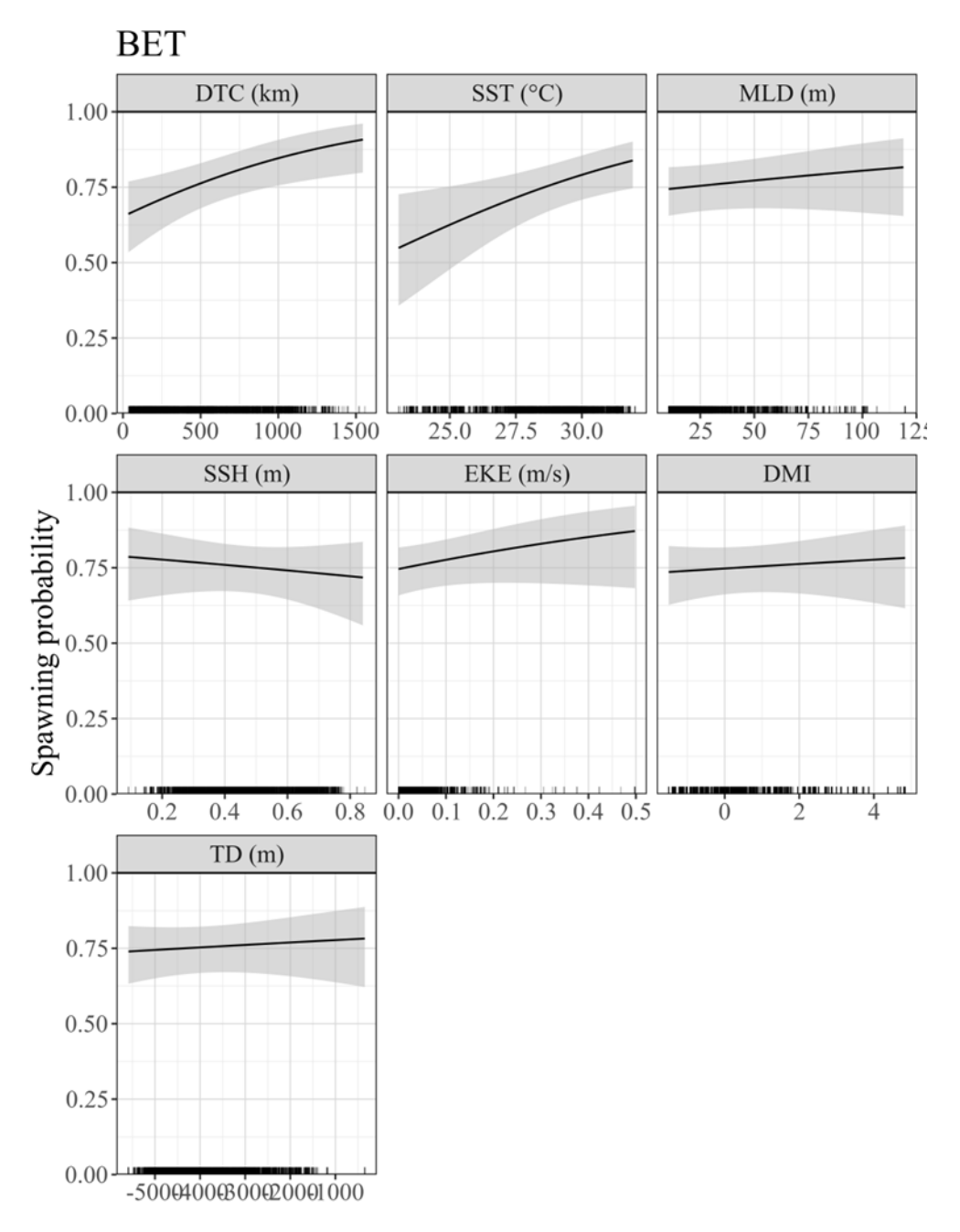


Figure 14 Partial effects of habitat covariates on the spawning probability of bigeye tuna in the Indian Ocean.

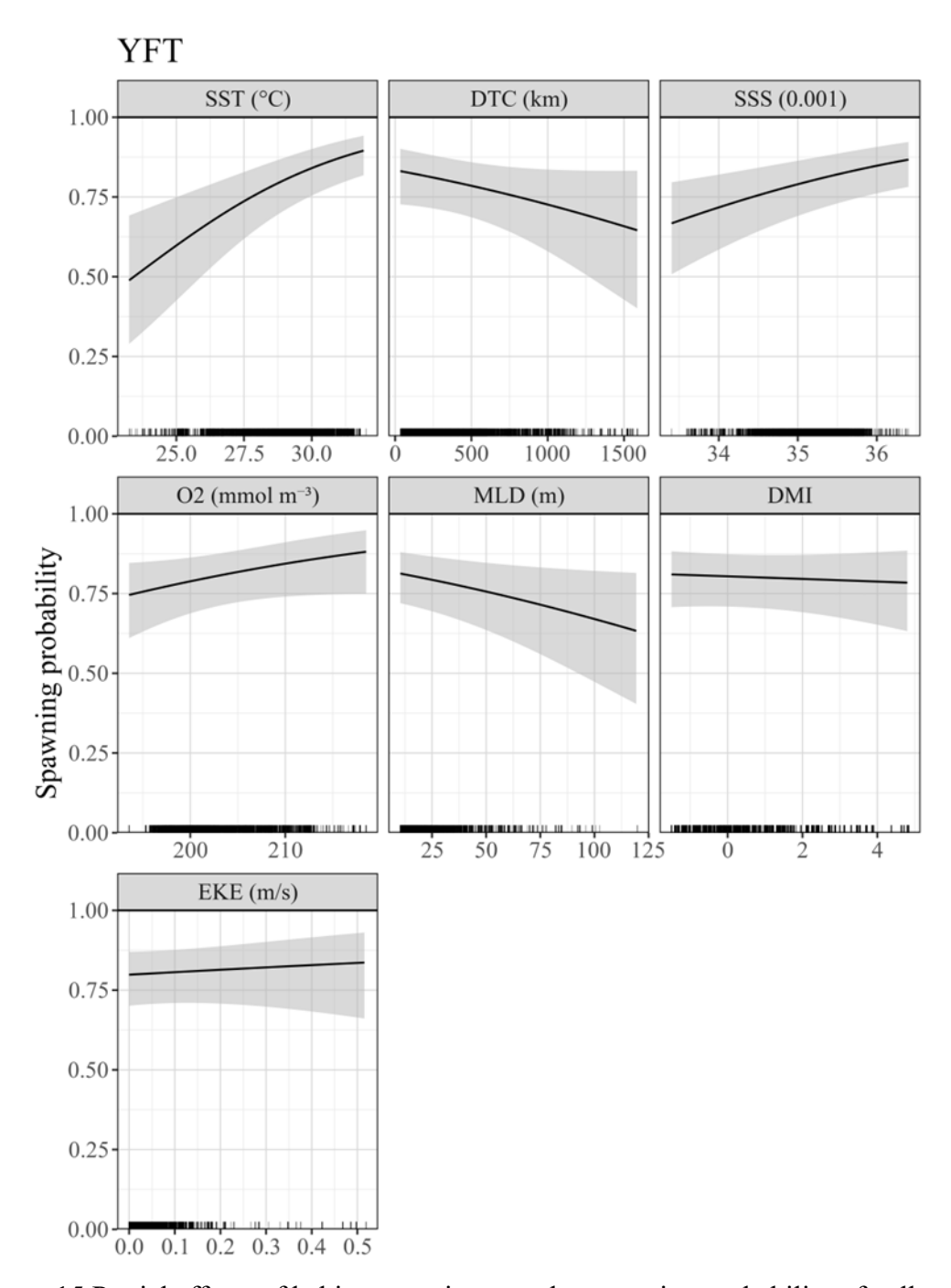


Figure 15 Partial effects of habitat covariates on the spawning probability of yellowfin tuna in the Indian Ocean.

# 7 Tables

Table 1: Code, description, class, and type of candidate explanatory variables. Catchability covariates were fixed at a specified value when predicting, while habitat covariates varied over space and time.

Code	Description	Class	Туре		
month	month	Factor (levels: 1,, 12)	-		
vessel	vessel id	Factor (levels: 1, 33)	Catchability		
n_prop	Proportion of nighttime fishing effort	Numeric	Catchability		
HBF	Hooks between float	Numeric	Catchability		
MLD	Mixing layer depth	Numeric	Habitat		
SST	Sea surface temperature	Numeric	Habitat		
SSS	Sea surface salinity	Numeric	Habitat		
SSH	Sea surface height	Numeric	Habitat		
EKE	Eddy kinetic energy	Numeric	Habitat		
CHL	Chlorophyll - a	Numeric	Habitat		
DO	Dissolved Oxygen	Numeric	Habitat		
DMI	Indian Ocean Dipole index	Numeric	Habitat		
DP	Ocean depth	Numeric	Habitat		
DTC	Distance to the coast	Numeric	Habitat		

Table 2 Parameters for the logistic regression model for estimating the fork length of female bigeye tuna and yellowfin tuna in the Indian Ocean at which 50% of the population is mature (L<sub>50</sub>, cm). a and  $\beta$  are the coefficients of the equation and L50 was computed as  $-a/\beta$  for the maturity threshold used: maturity stage over 3. Significant test shows the length-maturity relationship.

	Bigeye tun	Yellowfin tuna					
parameters	а	β	L <sub>50</sub>		а	β	L <sub>50</sub>
estimates	-12.473 0.114		109.3		-9.877	0.093	106.2
standard error	0.376 0.003		0.4		0.287	0.3	
significance			<i>p</i> < 0.001				

Table 3 VIF test for the variables in bigeye and yellowfin tuna model.

Bigeye tuna									Yellowfin tuna										
Variables	SST	EKE	SSH	DMI	Chla	DO	SSS	Depth	DTC	SST	Γ	EKE	SSS	SSH	DMI	Chla	DO	Depth	DTC
VIF	1.47	1.09	1.32	1.17	1.18		1.38	1.23	1.5	2.7		1.04	1.48	1.64	1.36	1.32	3.2	1.64	1.56

Table 4 Model selection and diagnostic results for bigeye and yellowfin tuna. M0: baseline model with month, vessel (as a random effect), and the spatial random field; M1: baseline model including environmental covariates; M2: baseline model including both catchability and habitat-related variables. Moran's I *p* values represent the significance of spatial autocorrelation of model residuals.

		BET					YFT		
	Convergency	df	Moran's I <i>p</i> value	AIC		Convergency	df	Moran's I p value	AIC
M0	Yes	15		8483.76	M0	Yes	15		10409.74
M1	Yes	23		8439.61	M1	Yes	23		10351.26
M2	Yes	25	0.343	8328.84	M2	Yes	26	0.661	10324.62